AGU PUBLICATIONS

Space Weather

RESEARCH ARTICLE
10.1002/2016SW001554

Key Points:
- We explain the lack of scintillation activity prior to the Halloween storm in October 2003 in the Peruvian longitude sector
- We carried out a study which forecasts the occurrence of equatorial spread *F* (ESF), on a night-to-night basis, in five longitude sectors
- The overall forecasting success is greater than 80% for each of the five longitude sectors

Correspondence to:
R. J. Redmon,
rob.redmon@noaa.gov

Citation:
Anderson, D. N., and R. J. Redmon (2017), Forecasting scintillation activity and equatorial spread *F*, *Space Weather*, *15*, 495–502, doi:10.1002/2016SW001554.

Received 17 OCT 2016
Accepted 17 JAN 2017
Accepted article online 21 JAN 2017
Published online 10 MAR 2017

Forecasting scintillation activity and equatorial spread *F*

David N. Anderson[1] and Robert J. Redmon[2]

[1]CIRES and NOAA/SWPC, University of Colorado Boulder, Boulder, Colorado, USA, [2]NOAA/NCEI, Boulder, Colorado, USA

Abstract When transionospheric radio waves propagate through an irregular ionosphere with plasma depletions or "bubbles," they are subject to sporadic enhancement and fading, which is referred to as scintillation. Communication and navigation systems may be subject to these detrimental effects if the scintillation is strong enough. It is critical to have knowledge of the current ionospheric conditions so that system operators can distinguish between the natural radio environment and system-induced failures. In this paper we briefly describe the Forecasting Ionospheric Real-time Scintillation Tool UHF scintillation forecasting technique, which utilizes the observed characteristic parameter $h'F$ from a ground-based, ionospheric sounder near the magnetic equator. The prereversal enhancement in vertical $E \times B$ drift velocity after sunset is the prime driver for creating plasma depletions and bubbles. In addition, there exists a "threshold" in the $h'F$ value at 1930 LT, $h'F_{thr}$, such that, on any given evening, if $h'F$ is significantly above $h'F_{thr}$, then scintillation activity is likely to occur, and if it is below $h'F_{thr}$, scintillation activity is unlikely to occur. We use this technique to explain the lack of scintillation activity prior to the Halloween storm in October 2003 in the Peruvian longitude sector. In addition, we have carried out a study which forecasts the occurrence or nonoccurrence of equatorial spread *F* (ESF), on a night-to-night basis, in five longitude sectors. The overall forecasting success is greater than 80% for each of the five longitude sectors.

1. Introduction

The paper by *Balsley et al.* [1972] entitled "Equatorial Spread *F*: Recent Observations and a New Interpretation" identified the collision-dominated Rayleigh-Taylor instability mechanism that would provide the primary plasma density irregularities that could account for most of the observed properties. The model suggested by *Balsley et al.* [1972] and extended by *Haerendel* [1972] incorporated flux tube integrated quantities in the expression for the Rayleigh-Taylor instability growth rate. The Rayleigh-Taylor mechanism was capable of accounting for (1) the close correlation with the height of the bottom of the *F* layer; (2) the fact that plasma irregularities appear both below and above the *F* layer height; and (3) the persistence of irregularities to be observed after downward *F* layer $E \times B$ drifts had commenced. This study essentially paved the way for both collision-dominated linear and nonlinear studies and collisionless Rayleigh-Taylor instability investigations.

It has long been appreciated that the rapid postsunset rise of the equatorial *F* region is the single most important parameter controlling the onset of scintillation activity and Equatorial Spread *F* (ESF) [*Booker and Wells*, 1938; *Farley et al.*, 1970; *Ossakow*, 1981; *Rastogi*, 1980; *Abdu et al.*, 1983; *Kelley and Maruyama*, 1992; *Jayachandran et al.*, 1993; *Sultan*, 1996]. The height rise is primarily due to the prereversal enhancement (PRE) in upward $E \times B$ drift velocity. *Fejer et al.* [1999] studied the effects of vertical plasma drift and the generation and evolution of ESF between 1968 and 1992 using the Jicamarca incoherent scatter radar in the Peruvian longitude sector. They find that when the $E \times B$ drifts are large enough, the necessary seeding mechanisms for generating strong ESF are always present. The threshold drift velocity to produce scintillation activity increases with increasing solar flux, and the largest drift velocities occur during the equinox and December solstice periods and the lowest occur in the June solstice period.

A measure of the strength of scintillation activity is given by the *S*4 index. This is an index that measures amplitude scintillation of the radio signals that pass through ionospheric irregularities. It is defined as root-mean-square of the signal intensity at the radio receiver. The Air Force Research Laboratory has established a network of UHF receivers called the SCItillation Netwok Decision Aid (SCINDA). These receivers record the signal amplitude and phase of radio signals sent out by the FleetSat geostationary satellites.at a number of different longitudes [*Groves et al.*, 1997]. In the Jicamarca, Peru longitude, these receivers are placed at Ancon, Peru, facing the east and west directions and provide the UHF *S*4 values as a function of time.

Caton and Groves [2006] developed a new index they term the total hourly mean *S*4 index (THMS4). This is the sum of the hourly mean *S*4 values over a 5 h period starting just after sunset. *Redmon et al*. [2010] incorporate the Ancon THMS4 values in developing their Forecasting Ionospheric Real-time Scintillation Tool (FIRST) technique that will be described in the next section.

In the following sections, we present (1) a brief description of the Forecasting Ionospheric Real-time Scintillation Tool (FIRST) concept; (2) the application of the FIRST technique to account for the lack of equatorial scintillation activity prior to the October 2003 Halloween storm, (3) the use of FIRST to forecast the day-to-day occurrence of equatorial spread *F* (ESF) in five longitude sectors; and (4) discussion and future work

2. FIRST Concept

The FIRST technique develops the capability to forecast regional UHF scintillation activity and ESF, on a night-to-night basis, through the use of ground-based ionospheric sounder observations near the magnetic equator. The UHF scintillation forecasting technique is described in a paper by *Redmon et al*. [2010] entitled "A Forecasting Ionospheric Real-time Scintillation Tool (FIRST)." The technique utilizes the observed characteristic parameter $h'F$ from a ground-based, ionospheric sounder near the magnetic equator. This paper demonstrated that there exists an excellent correlation ($R^2 \sim 0.91$) between $h'F$(1930 LT) and the prereversal enhancement in vertical $E \times B$ drift velocity after sunset which is the prime driver for creating plasma depletions and bubbles. In addition, there exists a "threshold" in the $h'F$ value at 1930 LT, $h'F_{thr}$, such that on any given evening, if $h'F$ is significantly above $h'F_{thr}$, then scintillation activity is likely to occur and if it is below $h'F_{thr}$, scintillation activity is unlikely to occur. The FIRST technique is applied to explain the absence of scintillation activity prior to the Halloween storm in the next section and, for the first time, to validate this technique at other longitude sectors in the subsequent section.

3. Scintillation Activity Prior to the Halloween Storm

We have applied the FIRST technique to explain the observed lack of equatorial scintillation activity in the Peruvian longitude sector prior to the 2003 Halloween storm. The primary factor for the decrease in scintillation activity is the increase in the solar flux and consequently the $F_{10.7}$ cm flux values. Between 5 and 19 October, the $F_{10.7}$ cm flux was about 100. Starting around 19 October, the $F_{10.7}$ flux begins increasing linearly and reaches a maximum value of 275 on 2 November before starting to decline. Since one of the important conclusions coming from the FIRST study demonstrated that the "threshold" in $h'F$(1930) increased with increasing $F_{10.7}$ cm flux, the observation that $F_{10.7}$ increases from 100 to 275 between 19 October and 2 November, means that $h'F_{thr}$ increased from 300 km altitude to 500 km altitude. We plot in Figure 1 the $F_{10.7}$ cm flux between 5 October and 6 November 2003 and the estimated $h'F_{thr}$ altitudes between these dates. In addition for this period, we plot the $h'F$(1930 LT) values observed by the Jicamarca digital sounder and the THMS4 values observed by the Ancon SCINDA receiver looking west.

Beginning on 18 October (day 291) with the $h'F_{thr}$ beginning to increase, the daily $h'F$(1930) values start to fall below the $h'F_{thr}$ values. Not surprisingly, the THMS4 values are equal to 0. Between days 291 and 307 (3 November) there are 11 days when THMS4 is 0 and 3 days when THMS4 is 1 or greater. Prior to day 291, the daily $h'F$(1930) values are predominately above the $h'F_{thr}$ values. During this period, there are 6 days when THMS4 is 1 or greater and 2 days when it is 0. It is well known that during solar maximum years when $F_{10.7}$ cm flux is high, the prereversal enhancement (PRE) in postsunset, vertical $E \times B$ drift velocities are significantly greater than the PRE values during solar minimum years [*Scherliess and Fejer*, 1999]. The fact that the PRE values do not track the rising $F_{10.7}$ cm flux values prior to the Halloween storm implies that there is some other mechanism that is inhibiting the PRE values from increasing. The inhibiting mechanism that affects the PRE response maybe associated with the change in geomagnetic activity that is occurring at the same time. The daily *Ap* values will reflect the changing geomagnetic activity since they are related to the 3-hourly *Kp* values for that day. Between 5 and 13 October, *Ap* is low. Between 14 and 22 October, *Ap* is moderate (*Kp* values are 4 to 5) and then after 22 October, *Ap* values are low again until the Halloween storm commences on 28 October. It is interesting to note that just when $F_{10.7}$ flux values begin to increase, $h'F$(1930) values start to decrease on 16

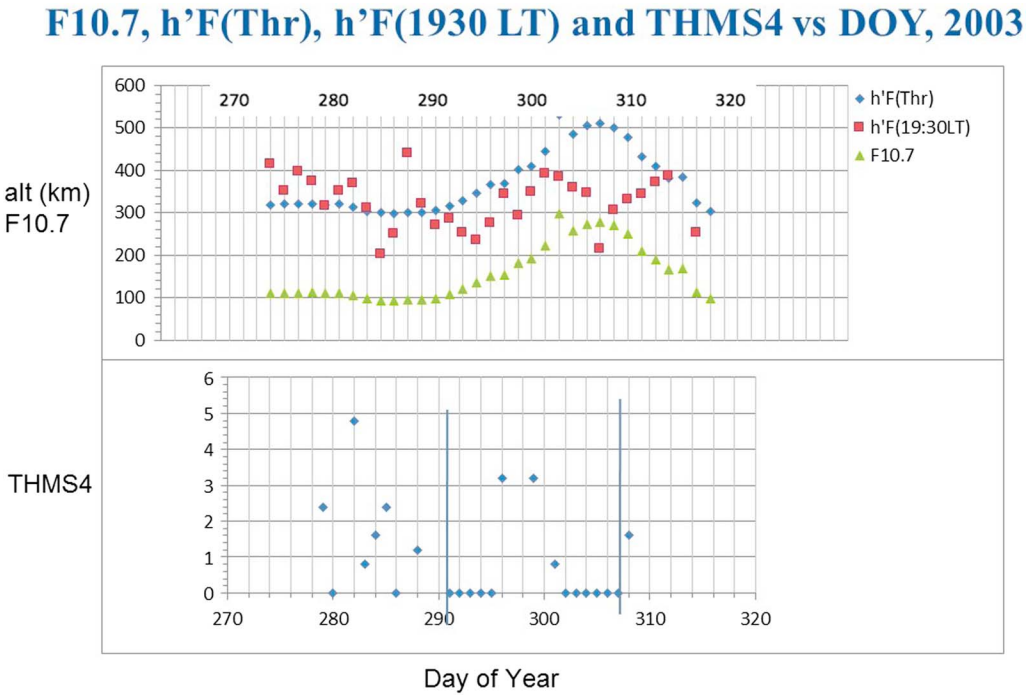

Figure 1. $F_{10.7}$ cm flux, $h'F$(thr), $h'F$(1930 LT), and THMS4 values from 2 October to 18 November 2003 (see text for details).

October for 4 days, thus falling below the $h'F_{thr}$ values. In a recent paper by *Carter et al.* [2014a] that analyzes the quiet-time, day-to-day variability in the formation of postsunset equatorial plasma bubbles (EPB) in the Southeast Asian region, they find that small changes in *Kp* strongly influences the daily EPB occurrence variability. When *Kp* increases, the high-latitude processes of changing neutral wind patterns (disturbance dynamo mechanism) cause the low-latitude, postsunset PRE to decrease and this decreases the EPB occurrence frequency. In a subsequent paper, *Carter et al.* [2014b] found that the Thermosphere, Ionosphere,

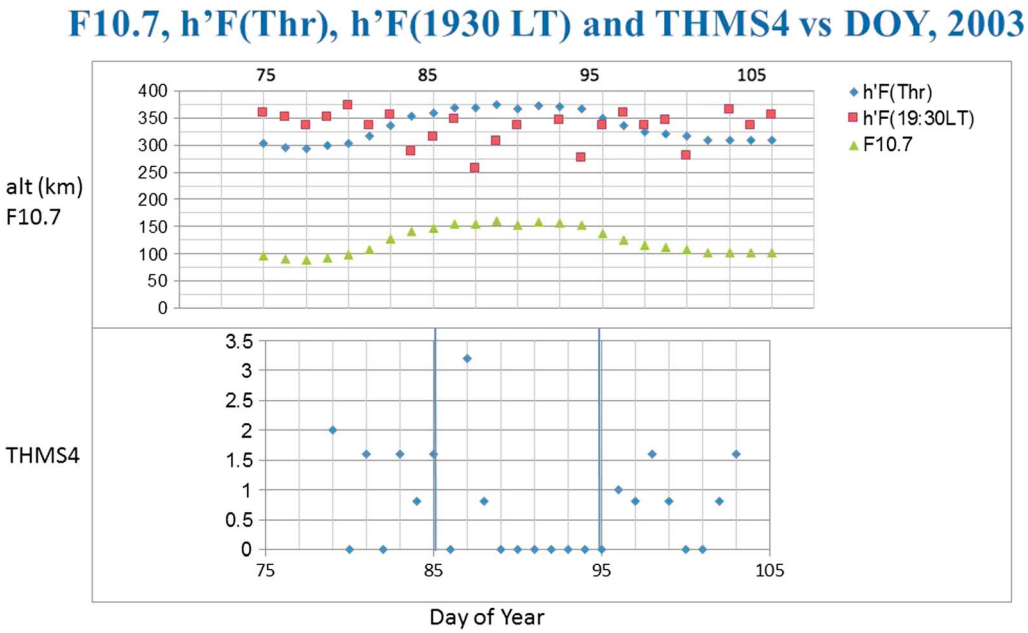

Figure 2. Same as Figure 1 but from 16 March to 16 April 2003.

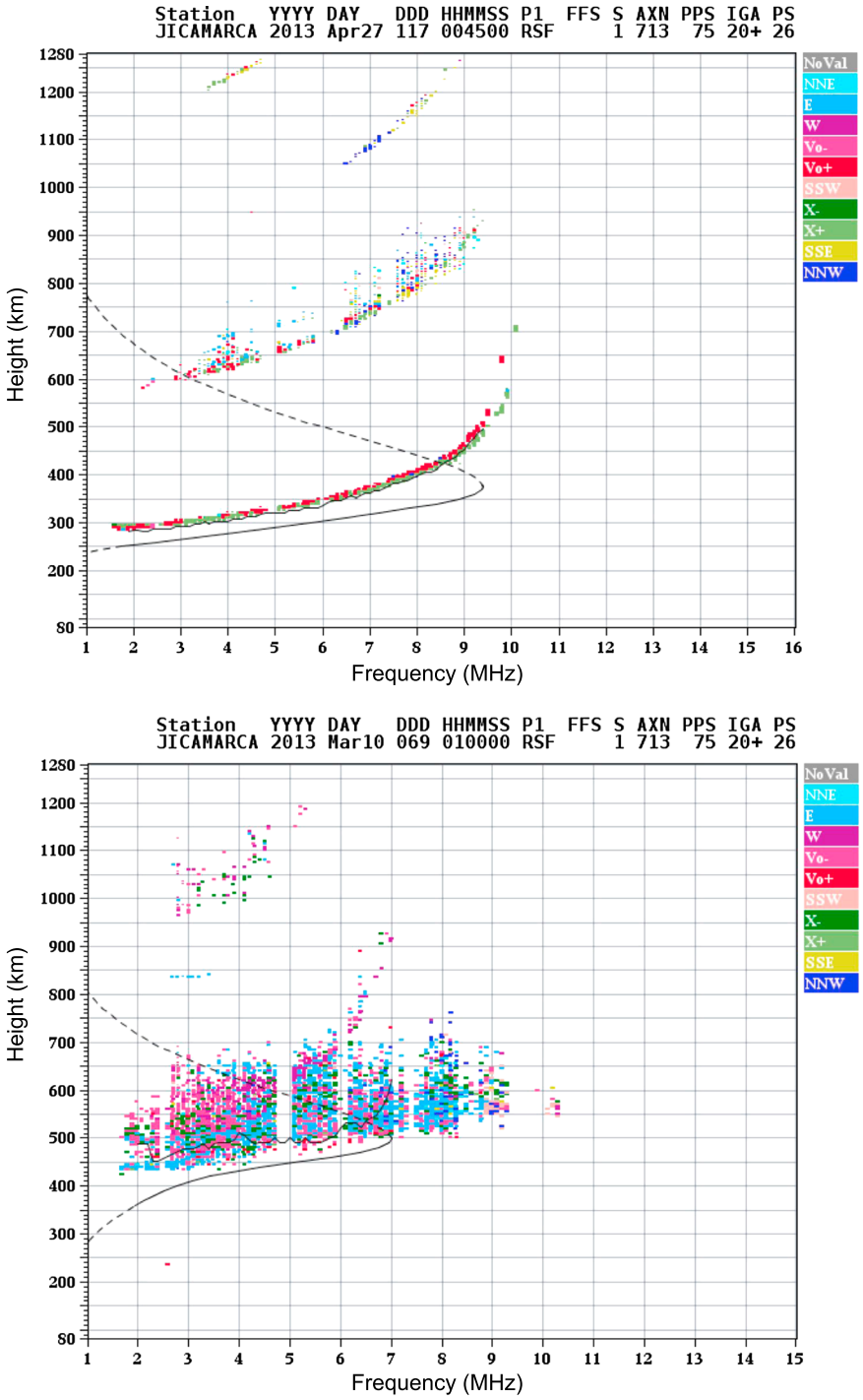

Figure 3. An example of (left) no spread *F* at Jicamarca on 27 April 2013 and (right) strong spread *F* at Jicamarca on 10 March 2013.

Electrodynamic General Circulation Model is capable of identifying days when EPB development, determined from calculated Rayleigh-Taylor growth rate, is suppressed as a result of geomagnetic activity. Interestingly enough, DMSP F14 and F15 SSIES observations from 18 to 28 October 2003 indicate, globally, that the occurrences of equatorial plasma bubbles (EPBs) were much fewer than climatology (B. Burke, private communication, 2010). Another index that is a measure of geomagnetic storm and substorm activity is the auroral electrojet (*AE*) index (http://wdc.kugi.kyoto-u.ac.jp). For the

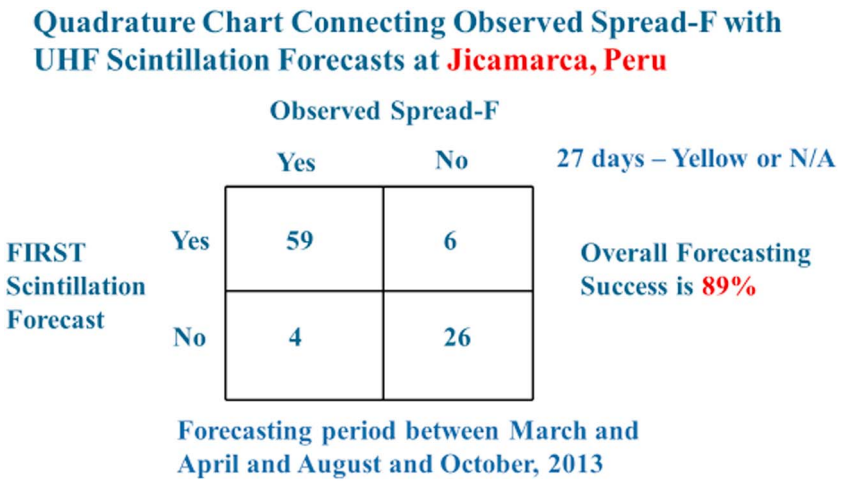

Figure 4. Quadrature chart for Jicamarca, Peru.

dates in Figure 1, the *AE* index also appears to be associated with the $h'F(1930)$ variations and hence the THMS4 values. The time variation in all of these indices and the $h'F(1930)$ values during this period confirm the findings of *Carter et al.* [2014a].

During a nonstorm period between 16 March and 15 April 2003, the $F_{10.7}$ cm flux increased from about 100 up to 150, remained at this value for about 8 days before decreasing back to 100. We carry out the same study we have described above for the Halloween storm. The results are displayed in Figure 2. An increase in $F_{10.7}$ cm flux from 100 to 150 implies an increase in $h'F_{thr}$ from 300 to 370 km altitude. Before day 85 (26 March), the daily $h'F(1930)$ primarily lies above $h'F_{thr}$ and THMS4 values are primarily above 0. Between days 85 and 95, $h'F(1930)$ values lie below $h'F_{thr}$, and there are 8 days when THMS4 values are 0 and only 2 when they are nonzero. After day 95 when $h'F(1930)$ once again is greater than $h'F_{thr}$, THMS4 values return to nonzero values. Similar to the period prior to the Halloween storm, it appears that an increase in geomagnetic activity may explain the reason why $h'F(1930)$ drops below $h'F_{thr}$ between days 85 and 95. Prior to day 85, *Ap* was below 10 for days 83 and 84 and between days 85 and 95, *Ap* increased to the 20s and 30s. After day 95, *Ap* again decreased to below 10 for days 96 and 97. These observations seem to confirm the findings of *Carter et al.* [2014a] that *Kp* can be responsible for day-to-day variability in scintillation activity even for the nonstorm period. The *AE* index for the dates in Figure 2 also confirms the association between *AE* index and $h'F(1930)$ and THMS4 values.

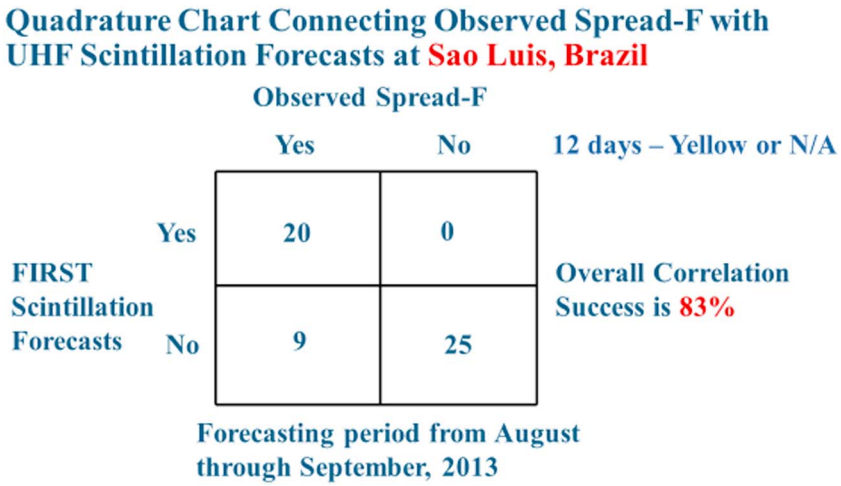

Figure 5. Quadrature chart for Sao Luis, Brazil.

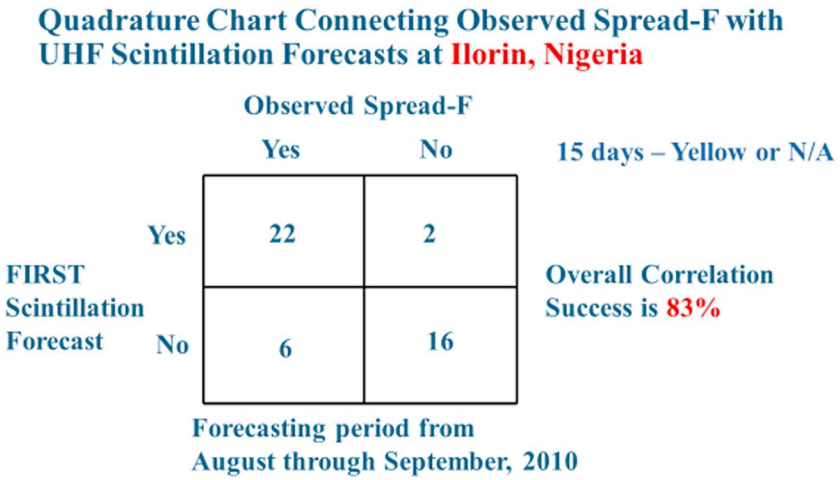

Figure 6. Quadrature chart for Ilorin, Nigeria.

4. Observations in Five Longitude Sectors

In this section, we present results that, for the first time, validate the FIRST technique in forecasting scintillation activity and equatorial spread *F* (ESF) in longitude sectors other than the Peruvian sector. The other four longitudes are at Sao Luis, Brazil; Ilorin, Nigeria; Guam; and the Kwajalein Atoll. The months that are chosen for each longitude sector are primarily chosen as transition months—a month where there is, generally, an absence of ESF to a month where, typically, ESF occurs. In this way, we hope to apply the forecasting technique to an equal number of days when ESF occurs and does not occur. We emphasize that this is not a seasonal/longitudinal study of ESF occurrence frequency but a validation of the FIRST forecasting technique at different longitude sectors. For the interested reader, there are two excellent articles that address the monthly/seasonal/longitudinal variations of equatorial irregularities: (1) The longitudinal morphology of equatorial *F* layer irregularities relevant to their occurrence [*Aarons*, 1993] and (2) On monthly/seasonal/longitudinal variations of equatorial irregularity occurrences and their relationship with the postsunset vertical drift velocities [*Su et al*., 2008].

In forecasting the occurrence or nonoccurrence of ESF in the five longitude sectors, there are four assumptions that are made. These are as follows: (1) If $h'F$ is **Less** than ($h'F_{thr}-10$ km) at 1930 LT, forecast is *No ESF*; (2) If $h'F$ is *Greater* than ($h'F_{thr}+10$ km) at 1930 LT, forecast is *ESF Will Occur*; (3) No forecast is made if $h'F$ at 1930 LT is within ±10 km of $h'F_{thr}$; and (4) For each site, confirmation of the occurrence or

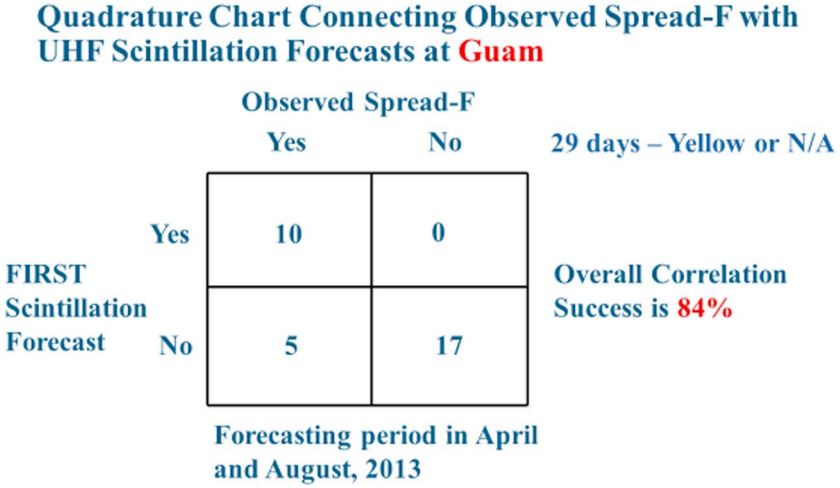

Figure 7. Quadrature chart for Guam.

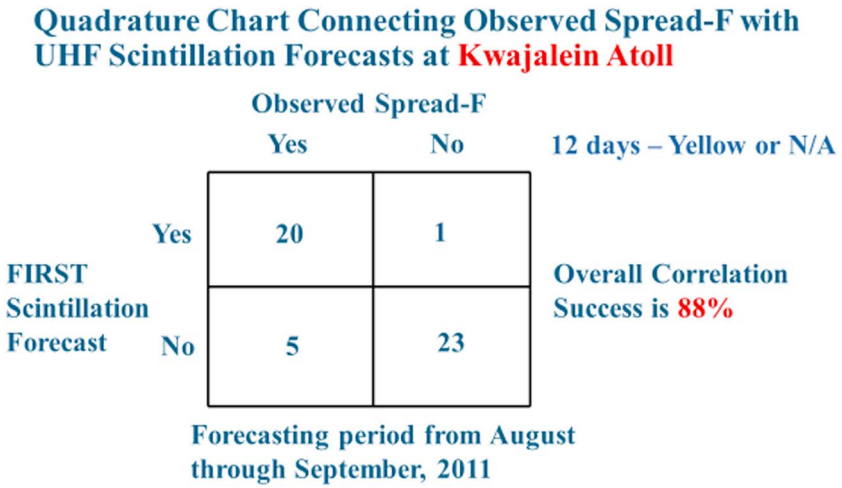

Figure 8. Quadrature chart for Kwajalein Atoll.

nonoccurrence of ESF is made at 2030 LT. In order to obtain a rough number of equal ESF occurrence and nonoccurrence days, the months chosen are transition months: (1) For Jicamarca, March and April and August through October 2013; (2) For Sao Luis, August through September 2013; (3) For Ilorin, August through September 2010; (4) For Guam, April and August 2013; and (5) For Kwajalein, August through September 2011. An example of a no ESF and a strong ESF day at Jicamarca is shown in Figure 3 for 27 April and 10 March 2013, respectively.

We present our results as quadrature charts for each of the five longitude sectors. In the Jicamarca, Peru sector, we examined the period from 1 March to 30 April and 15 August 15 to 15 October 2013. During this period there were 30 days where FIRST forecast no ESF, 65 days where FIRST forecast that ESF will occur, and 27 days where there were no data or $h'F$(1930 LT) was within ±10 km of $h'F$(thr). The quadrature chart is pictured in Figure 4.

In the Sao Luis, Brazil, longitude sector, the forecasting period was from 1 August to 30 September 2013. During this period, there were 20 days when ESF was forecast to occur, 34 days when the forecast was for no ESF, and 12 days where no data were available or $h'F$(1930 LT) was in the Yellow region. The quadrature chart for Sao Luis is shown in Figure 5.

The forecasting period for Ilorin, Nigeria, was from 1 August to 30 September 2010. During this period, FIRST forecast 24 days when ESF would occur and 22 days with no ESF. There were 15 days when no data were available or $h'F$(1930 LT) was in the Yellow region. The quadrature chart for Ilorin is shown in Figure 6.

For Guam, the forecasting period was April and August 2013. There were only 10 days during this period where FIRST could forecast the occurrence of ESF and 22 days when FIRST forecast no ESF. An unusually large number of days, 29, were either in the Yellow region or were not available. The Quadrature chart is show in Figure 7.

Finally, the forecasting period for Kwajalein Atoll was from August 1 through September 30, 2011. There were 21 days when FIRST forecast ESF would occur and 28 days when the forecast was for no ESF. There were 12 days when $h'F$ was in the Yellow zone or no data was available. The Quadrature chart is shown in Figure 8.

In each of the five longitude sectors, the Overall Correlation Success is greater than 80% which is significant and gives us confidence that the FIRST technique for forecasting ESF occurrence or nonoccurrence on a day-to-day basis is tractable. Although the observation periods were somewhat limited because the digital sounder observations in DidBase [*Reinisch and Galkin*, 2011] were limited, we feel the results are statistically significant.

5. Discussion and Future Work

In the first part of the paper we demonstrate the capability of FIRST to account for the lack of scintillation activity prior to the Halloween storm. As $F_{10.7}$ cm flux begins to increase, the $h'F$(1930) values begin falling

below the $h'F_{thr}$ values. We speculate that this may be due to the increase in geomagnetic activity that is occurring at this time which offsets the expected rise in PRE due to the increasing $F_{10.7}$ value. All of the indices, *Kp*, *Ap*, and *AE*, begin increasing after 16 October 2003, and the $h'F$(1930) values begin decreasing below the $h'F_{thr}$ and THMS4 values go to 0. The same scenario plays out for the nonstorm period between 16 March and 15 April 2003 when the $F_{10.7}$ cm flux increases from 100 to 150 and back to 100. During the increase in $F_{10.7}$, $h'F$(1930) decreases and drops below $h'F_{thr}$ causing THMS to drop to 0. During this same time, *Ap* increases from below 10 to the 20s and 30s and then back to below 10. We again speculate that the increasing *Ap* values more than offset the increasing PRE due to increasing $F_{10.7}$ values. This behavior seems to confirm the results presented by *Carter et al*. [2014a] for the Asian sector.

In the second part of the paper, we estimate the overall success in using FIRST to forecast the day-to-day occurrence of ESF in five different longitude sectors. In one of the assumptions, we excluded days $h'F$(1930 LT) was within ±10 km of $h'F_{thr}$. This assumption excluded a significant number of days; however, since the severity of ESF was not quantified on a day-to-day basis, excluding this region seems justified. Our determination of an "overall success" value is "qualified" by this assumption. Even so, an overall correlation success of greater than 80% in all five longitude sectors demonstrates an impressive predictive capability of the FIRST technique to forecast ESF on a day-to-day basis.

Given the success of this study, there may be justification for developing a real-time ESF forecasting product if there exist a number of real-time digital sounder observations on the magnetic equator. Currently, the only DidBase, real-time sounders exist at Jicamarca, Peru; Sao Luis, Brazil; and Guam. At SWPC and NCEI we plan to investigate the possibility of developing a real-time ESF product that would be available to all navigation and communication customers.

Acknowledgments
The authors wish to thank Ivan Galkin at the Global Ionospheric Radio Observatory (GIRO) at Lowell Digisonde International (LDI) and GIRO principal investigator, and B. W. Reinisch of the University of Massachusetts Lowell for making these data files available (http://giro.uml.edu/).

References

Aarons, J. (1993), The longitudinal morphology of equatorial *F*-layer irregularities relevant to their occurrence, *Space Sci. Rev.*, *63*, 209, doi:10.1007/BF00750769.

Abdu, M. A., R. T. Demedeiros, J. A. Bittencourt, and I. S. Batista (1983), Vertical ionospheric drift velocities and range type spread-*F* in the evening equatorial ionosphere, *J. Geophys. Res.*, *88*(NA1), 399–402, doi:10.1029/JA088iA01p00399.

Balsley, B. B., G. Haerendel, and R. A. Greenwald (1972), Equatorial spread F: Recent observations and a new interpretation, *J. Geophys. Res.*, *77*(28), 5625–5628, doi:10.1029/JA077i028p05625.

Booker, H. G., and H. W. Wells (1938), Scattering of radio waves by the *F*-region ionosphere, *Terr. Magn. Atmos. Electr.*, *43*(3), 249–256, doi:10.1029/TE043i003p00249.

Carter, B. A., E. Yizengaw, J. M. Retterer, M. Francis, M. Terkildsen, R. Marshall, R. Norman, and K. Zhang (2014a), An analysis of the quiet time day-to-day variability in the formation of post-sunset equatorial plasma bubbles in the Southeast Asian region, *J. Geophys. Res. Space Physics*, *119*, 3206–3223, doi:10.1002/2013JA019570.

Carter, B. A., et al. (2014b), Geomagnetic control of equatorial plasma bubble activity modeled by TIEGCM with *Kp*, *Geophys. Res. Lett*, *41*, 5331–5339, doi:10.1002/2014GL060953.

Caton, R., and K. Groves (2006), Longitudinal correlation of equatorial ionospheric scintillation, *Radio Sci.*, *41*, RSSS22, doi:10.1029/2005RS003357.

Farley, D. T., B. B. Balsley, R. F. Woodman, and P. McClure (1970), Equatorial spread-*F*—Implications of VHF radar observations, *J. Geophys. Res.*, *75*(34), 7199–7216, doi:10.1029/JA075i034p07199.

Fejer, B. G., L. Scherliess, and E. R. de Paula (1999), Effects of the vertical plasma drift velocity on the generation and evolution of equatorial spread *F*, *J. Geophys. Res.*, *104*(A9), 19,859–19,869, doi:10.1029/1999JA900271.

Groves, K. M., et al. (1997), Equatorial scintillation and systems support, *Radio Sci.*, *32*(5), 2047–2064, doi:10.1029/97RS00836.

Haerendel, G. (1972), Rayleigh-Taylor instability as cause of equatorial spread-*F*, *Trans. Am. Geophys. Union*, *53*(11), 1082.

Jayachandran, B., N. Balan, P. B. Rao, J. H. Sastri, and G. J. Bailey (1993), HF Doppler and ionosonde observations on the onset conditions of equatorial spread *F*, *J. Geophys. Res.*, *98*(A8), 13,741–13,750, doi:10.1029/93JA00302.

Kelley, M. C., and T. Maruyama (1992), A diagnostic model for equatorial spread-*F*. 2. The effect of magnetic activity, *J. Geophys. Res.*, *97*(A2), 1271–1277, doi:10.1029/91JA02607.

Ossakow, S. L. (1981), Spread-F theories—A review, *J. Atmos. Terr. Phys.*, *43*(5/6), 437–452.

Rastogi, R. G. (1980), Seasonal-variation of equatorial spread-F in the American and Indian Zones, *J. Geophys. Res.*, *85*(NA2), 722–726, doi:10.1029/JA085iA02p00722.

Redmon, R. J., D. Anderson, R. Caton, and T. Bullett (2010), A Forecasting Ionospheric Scintillation Tool (FIRST), *Space Weather*, *8*, S12003, doi:10.1029/2010SW000582.

Reinisch, B. W., and I. A. Galkin (2011), Global ionosphere radio observatory (GIRO), *Earth Planets Space*, *63*, 377–381, doi:10.5047/rpd2011.03.001.

Scherliess, L., and B. G. Fejer (1999), Radar and satellite global equatorial *F* region vertical drift model, *J. Geophys. Res.*, *104*(A4), 6829–6842, doi:10.1029/1999JA900025.

Su, S.-Y., C. K. Chao, and C. H. Liu (2008), On monthly/seasonal/longitudinal variations of equatorial irregularity occurrences and their relationship with the postsunset vertical drift velocities, *J. Geophys. Res.*, *113*, A05307, doi:10.1029/2007JA012809.

Sultan, P. J. (1996), Linear theory and modeling of the Rayleigh-Taylor instability leading to the occurrence of equatorial spread F, *J. Geophys. Res.*, *101*(A12), 26,875–26,891, doi:10.1029/96JA00682.